Sensors and Materials, Vol. 28, No. 2 (2016) 163–171
MYU Tokyo

S & M 1166

Effect of Vacuum Annealing on Tensile Mechanical Characteristics of Au Bonding Wires

Akio Takagi, Takaaki Kato,[1] Shugo Miyake,[1] Shozo Inoue, and Takahiro Namazu*

Department of Mechanical Engineering, University of Hyogo,
2167 Shosha, Himeji, Hyogo 671-2201, Japan
[1]Kobelco Research Institute Inc.,
1-5-5 Takatsukadai, Nishi-ku, Kobe, Hyogo 651-2271, Japan

(Received August 6, 2015; accepted November 2, 2015)

Keywords: Au bonding wire, tensile test, Young's modulus, yield strength, annealing, grain growth

In this paper, the effect of vacuum annealing on the mechanical properties of Au bonding wires is described. Au bonding wires with a diameter of 25 μm are subjected to quasi-static uniaxial tensile tests in laboratory air. The bonding wire specimens are prepared by attaching a wire to a Si frame fabricated by deep reactive ion etching (DRIE). The mean Young's modulus and 0.2% offset yield strength are 114 GPa and 354 MPa, respectively. By annealing at 100–300 °C for 10 min in vacuum, Young's modulus gradually decreases with increasing annealing temperature, whereas yield strength rapidly decreases in the annealed wires at temperatures above 200 °C. The annealing effect is discussed on the basis of the change in the number of recrystallized grains in the wires.

1. Introduction

Bonding wires are one of the significant mechanical and electrical elements indispensable for semiconductor device packaging.(1) The use of bonding wires made of Au, copper, and aluminum, which are commonly used for ball-and-wedge bonding to mechanically and electrically connect a semiconductor device chip to a package, leads to the fabrication of the vast majority of integrated circuits (ICs). Recently, a "hyperfine" wire with a diameter smaller than 20 μm has been developed and utilized for ICs including narrow-pitch electrode pads. The largest advantage of such a wire is cost. A wire of some length should be cheaper than a courser wire of the same length because it contains less Au than the courser wire. Its disadvantage is weakness. Typically, because a bonding wire is used in a bent form, mechanical durability against bending is required for long-term reliability. In addition, typical semiconductor devices generate heat during operation because of Joule heating. The heat is considered to affect mechanical durability because the crystal grain of the wire changes in size and texture with temperature elevation. Therefore, the relationship between the amount of applied heat and mechanical reliability should be investigated experimentally to assess the lifetime of semiconductor devices.

The mechanical properties of bonding wires have so far been evaluated by uniaxial tensile tests. There are numerous technical reports describing the tensile and yield strengths.(2–8) The effect of annealing on these mechanical characteristics has also been reported.(6–8) However, discussions of

*Corresponding author: e-mail: namazu@eng.u-hyogo.ac.jp

ISSN 0914-4935

Young's modulus are scarce because precise measurement of the displacement of the bonding wire during the tests is required for the derivation of Young's modulus. In tensile tests for bonding wires, cross-head stroke of the tensile test equipment is used very often for specimen elongation, which is not ideal to accurately derive Young's modulus. In this study, we developed a uniaxial tensile test technique for Au bonding wires to accurately obtain the stress–strain relation for the derivation of Young's modulus and yield strength. The effect of vacuum annealing on these mechanical characteristics is discussed from the viewpoint of recrystallization.

2. Experimental Procedure

Figure 1 shows a schematic of the fabrication step for a Au bonding wire tensile test specimen together with photographs of the Si frame and alignment jig. A Au bonding wire with a diameter of 25 μm and a purity of 99.99% (Heraeus Deutschland GmbH & Co. KG) was chosen as a target material. First, the wire was cut to a length of roughly 10 cm. Ten bundled wires were annealed at 100, 200, and 300 °C for 10 min at 2.0×10^{-4} Pa. Then a wire was set onto a tensile test frame made of Si that was placed on a cemented carbide alignment jig (Step 1). The Si frame fabricated by deep reactive ion etching (DRIE) is composed mainly of two square holes in the fixed and movable parts and four Si springs supporting the movable part.[9–11] The alignment jig has two square convex structures with a slit, measuring 0.05 mm in width and 1.4 mm in depth, fabricated by wire discharge. The convex structures were put through two square holes of the Si frame before setting the Au bonding wire. The slit in the convex piece was used for the alignment between the longitudinal direction of the bonding wire and the tensile direction of the frame. After placing the

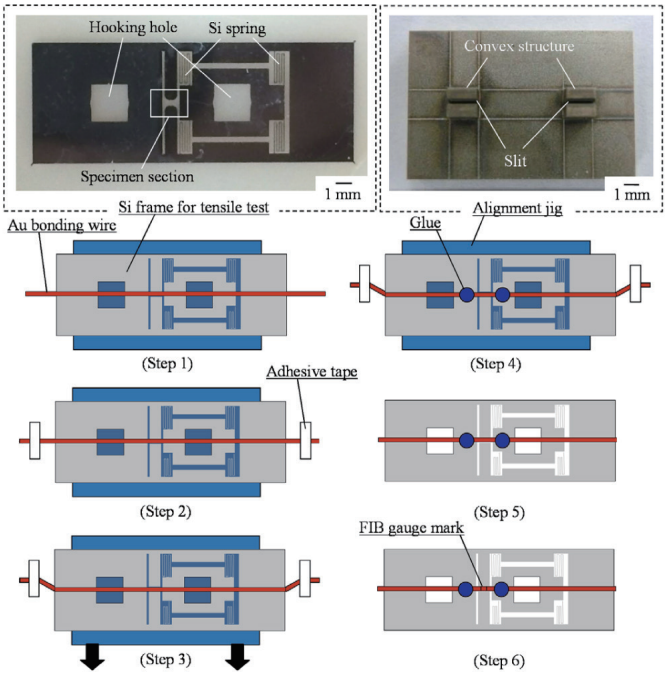

Fig. 1. (Color online) Schematic of process flow for fabricating Au bonding wire specimens for uniaxial tensile tests along with photographs of the Si frame and alignment jig.

bonding wire onto the Si frame, both ends of the wire were attached to a stage with adhesive tape (Step 2). Then both the frame and the cemented carbide jig were moved toward the transverse direction to tense the wire toward the tensile direction (Step 3). A strong instant adhesive was allowed to seep through sample stages of the Si frame to adhere the wire to the stages (Step 4). After keeping it intact for a day to desiccate it as completely as possible, the wire was cut in the vicinity of the attached adhesive tape (Step 5). After that, two gauge marks were fabricated onto the wire directly using focused ion beams (FIBs) with an acceleration voltage of 40 kV (Step 6). The distance between the two gauge marks was set to 500 μm. The etched depth was controlled to be less than 0.5 μm to avoid unwanted stress concentrations at the marks during the test. In our test equipment, the tensile displacement between two gauge marks was directly measured by an image processing system with a charge-coupled device (CCD) camera, which is described later.

Figure 2 shows a representative Au bonding wire specimen produced via the preparation steps described in Fig. 1. The bonding wire was set straightforwardly in the tensile direction. From the magnified picture, two gauge marks measuring approximately 5 μm in width and 23 μm in length were fabricated. We observed that these marks could be successfully detected with a CCD camera for specimen displacement measurement.

Figure 3 shows specially developed uniaxial tensile test equipment for minute specimens. With this equipment, we characterized various thin materials, such as single and polycrystalline Si, Si-related films, sputtered metal films, electroplated films, and polymers.[9–16] The equipment consists of a piezoelectric actuator, an actuator case, a load cell, a linear variable differential transformer (LVDT), a course stage, and specimen holders with a cartridge heater. The actuator case possesses a lever to amplify the actuator elongation by a factor of 4.1 in the tensile direction. The load cell

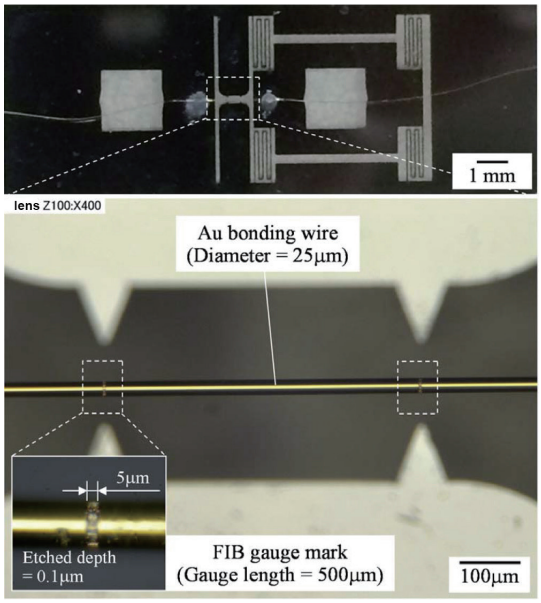

Fig. 2. (Color online) Photograph of the Au bonding wire specimen produced for a uniaxial tensile test along with the magnified picture of the wire with FIB-fabricated gauge marks.

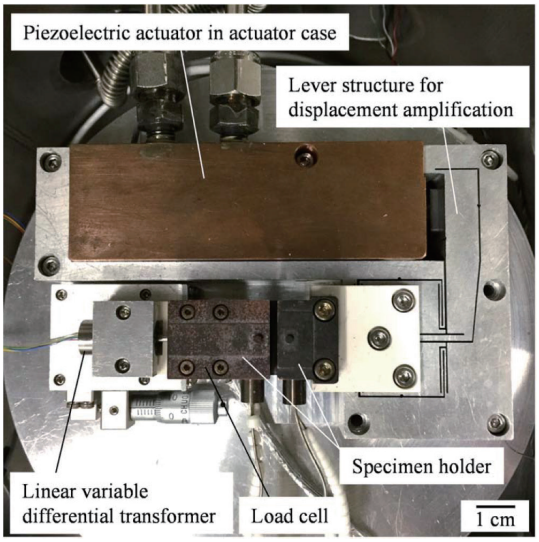

Fig. 3. (Color online) Specially developed uniaxial tensile test equipment. The equipment consists of a piezoelectric actuator, a load cell, a linear variable differential transformer, and a specimen holder.

has a resolution of 2 mN. The equipment is placed beneath a CCD camera in order to directly measure specimen elongation between two gauge marks without physical contact. In this system, the displacement is measured with a resolution of approximately 13 nm/pixel. The equipment may be operated in several test modes, including quasi-static tensile test, stress-relaxation test, creep test, and cyclic loading test modes.[9–18] Also, it is set in a vacuum chamber to do these tests in vacuum or inert gas as well as in ambient air. Test temperature is controlled within the range from room temperature to 300 °C. In this study, all the tests were carried out in the quasi-static tensile mode at a strain rate of 5.0×10^{-4} s^{-1} in ambient air. Temperature and humidity were not controlled.

3. Results and Discussion

Figure 4 shows representative nominal tensile stress–strain relationships for the unannealed and annealed Au bonding wires together with the magnified figure in the strain ranging from 0 to 0.2%. All the wires were tensioned to failure. No wires fractured at the gauge mark fabricated by FIBs. The stress–strain relationship for the unannealed wire is linear within the strain range from 0 to 0.5%. At around 0.5%, the wire yields to stress, and plastic deformation starts. At around 2.3%, the stress rapidly drops, and the wire fractures at 4.2%. The relationship for the 100 °C-annealed wire shows a somewhat similar shape to that for the unannealed wire. The plastic deformation range is larger by approximately 22% than the deformation range before annealing. In the 200 °C-annealed wires, however, three different stress–strain relationships were obtained. One of the 200 °C-annealed wires shows a similar stress–strain relationship to the unannealed and 100 °C-annealed wires [see 200 °C-annealed (A)]. After the maximum stress, stress drops to around 20 MPa, followed by failure. The stress–strain curves for the other two 200 °C-annealed wires [200 °C-annealed (B) and (C)] show a large difference compared with that for the 200 °C-annealed (A) wire. The 200 °C-annealed (B) and (C) wires fracture at the maximum tensile stress applied. These wires exhibit similar stress–strain relationships, but there are two different characteristics, namely, yield strength and breaking strain. The yield strengths of these wires are 150 and 85 MPa, which differ by 43%. The breaking strains are also different, 4.6 and 10.5%. For the 300°C-annealed wire, the stress–strain curve

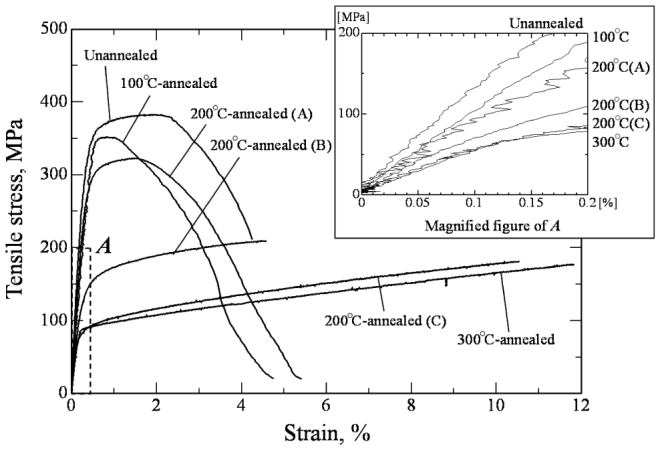

Fig. 4. Representative tensile stress–strain curves for Au bonding wire specimens. All the tests were conducted at room temperature in ambient air.

seems to be very similar to those for the 200 °C-annealed wires showing the lowest yield strength and highest breaking strain.

Figure 5(a) depicts the relationship between annealing temperature and Young's modulus. The Young's modulus for the unannealed Au bonding wire is 114 GPa on average, which is approximately 47% higher than the literature value of 80 GPa for bulk Au.[19] After vacuum annealing at 100 °C for 10 min, the mean value changed to 82 GPa, which is a 29% decrease from the mean value before annealing. With increasing temperature to 200 and 300 °C, the mean values gradually decrease to 72 and 55 GPa, respectively. The 300 °C-annealed wire's value is approximately 71% of the bulk value.[19] The data scatter of Young's modulus for the 200 °C-annealed wires is found to be the largest. The relationship between annealing temperature and yield strength shown in Fig. 5(b) shows a trend similar to that between annealing temperature and Young's modulus. Yield strength was defined as a 0.2% offset yield strength because all the Au bonding wires did not show yield points clearly. The yield strength of the unannealed wire is 354 MPa on average, which is roughly three times the literature values.[3–5] The yield strength does not change markedly even after annealing at 100 °C. The data scatter is found to increase after annealing. The yield strength markedly decreases with an increase in annealing temperature to 200 °C, where the mean value is 183 MPa, almost half of the value for the 100 °C-annealed wire. Note that the data scatter markedly increases at 200 °C. The standard deviation for the 200 °C-annealed wires is 82 MPa, which is approximately five times larger than that for the 100 °C-annealed wire. In the 300 °C-annealed wires, the yield strength and standard deviation decrease to 98 and 14 MPa, respectively.

To probe the cause of the annealing temperature effect, the cross-sectional observation of the Au bonding wires tested was conducted. Figure 6 shows representative cross-section photographs taken along the length of the wires. These cross sections were prepared by FIB fabrication along the center line of the wires. In the unannealed wire shown in Fig. 6(a), a line pattern along the length can be seen. In particular, the pattern is seen clearer around the core of the wire. The line width is roughly 300–500nm. Each line represents a columnar crystal structure derived by wire fabrication. Au bonding wires are typically produced by multiple drawing and annealing

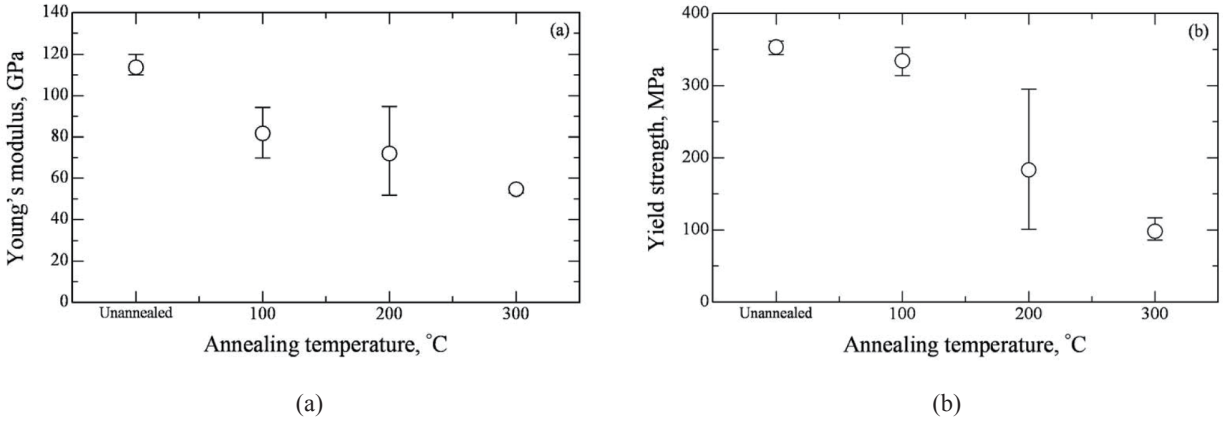

(a) (b)

Fig. 5. Effect of annealing temperature on mechanical properties of Au bonding wire: (a) Young's modulus and (b) yield strength.

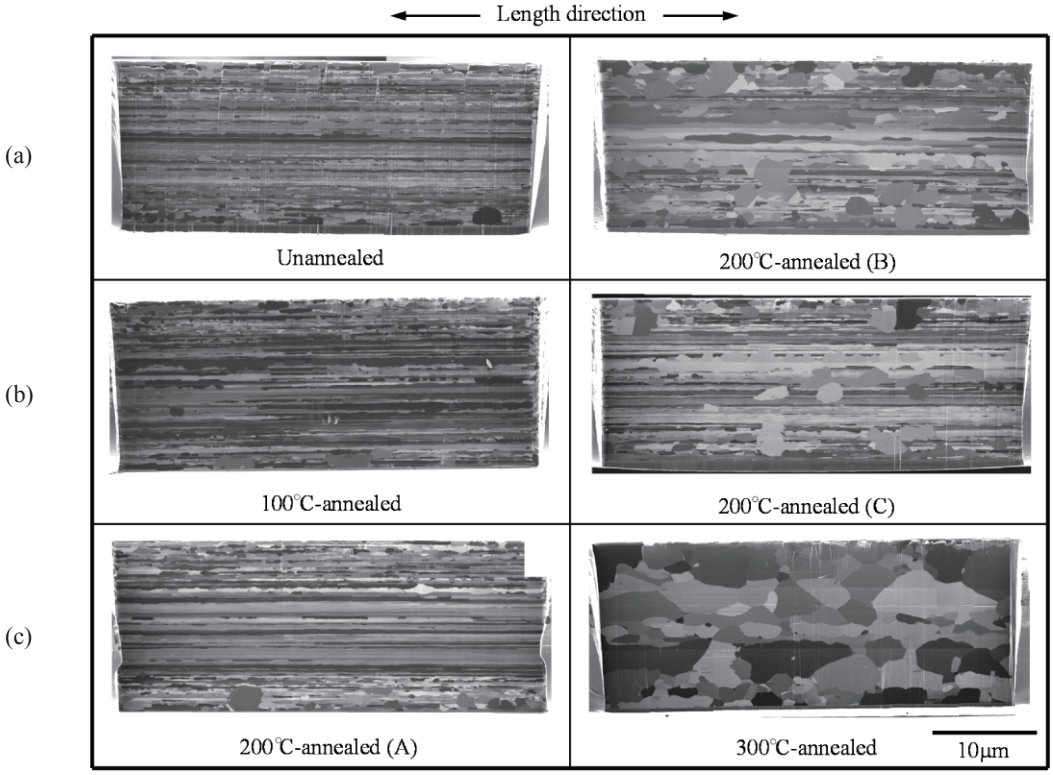

Fig. 6. Representative cross-sectional observations of Au bonding wires. The unannealed wire has a columnar crystal structure along its length. In the annealed wires, the number of recrystallized grains increases with annealing temperature elevation.

processes.[20] The grain size and texture depend on these processes. The columnar structure is strongly derived from drawing, which definitely strengthens the wires.[5,21] In the Young's modulus and yield strength, the large differences between experimentally obtained and literature values could have been caused by the drawing process effect. In the portion close to the wire surface, there are spherical crystal grains with diameters of 100–300 nm. These may possibly be associated with the local temperature increase around the wire surface during wire forming. In the 100 °C-annealed wire shown in Fig. 6(b), a columnar crystal pattern still remains. By annealing, it seems that no significant changes in texture were produced, except that small spherical grains might have grown. In the 200 °C-annealed wires, the number of spherical grains grown by annealing increases compared with that in the 100 °C-annealed wire. Spherical grains can be found in the vicinity of the wire surface. Note, however, that in the wires annealed at 200 °C, the number of grains differs. In Fig. 6(c), the cross-sectional image looks similar to the image of the 100 °C-annealed wire, although several large grains that were not observed previously appear after 200 °C annealing. The grains grew in only the vicinity of the surface, which indicates that the surface is easily affected by the heat during annealing. In Fig. 6(d), the number of spherical grains grown with diameters of 2–3 μm increases compared with that in the wire in Fig. 6(c). Several grown grains are found in the inside of the wire as well as in the vicinity of the surface. In Fig. 6(e), there are many more spherical grains in the entire wire. Despite the same annealing temperature of 200 °C, the reason

why the number of spherical grains grown differs is probably related to the fact that the annealing temperature is very close to the recrystallization temperature for Au.[22] Because of the ten bundled wires during annealing, the individual differences in the degree of annealing are small. The wire annealed at 300 °C, as shown in Fig. 6(f), is composed of only spherical grains, and no columnar structure along the length direction appears. This indicates that the entire wire was recrystallized during annealing at 300 °C.

Figure 7(a) shows the relationship between recrystallized grain percentage and Young's modulus. The grain percentage was defined as a percentage of recrystallized spherical grain area in the entire cross-sectional area produced by FIB fabrication. The calculation was carried out using a binary image processing technique.[23] At the lowest spherical grain percentage, Young's modulus is 114 GPa on average. With increasing grain percentage, the modulus gradually decreases. Even though the grain percentage is 100%, however, a modulus of 55 GPa deviates by 31% from the literature value of 80 GPa for bulk Au.[19] There are many reports of the mechanical characteristics of Au bonding wires,[3–7] Au nanowires,[24–26] Au thin films,[27–29] and Au bulk,[19] where Young's modulus ranges from 35 to 140 GPa. These values are strongly dependent on the grain size and texture that are determined by the fabrication process, annealing conditions, and surface treatment conditions. Further investigation, such as grain size measurement or crystal orientation determination, is required in the future, in order to explain the difference in Young's modulus between experiments and literature works.

Figure 7(b) represents the relationship between recrystallized grain percentage and yield strength. The yield strength monotonically decreases with an increase in recrystallized grain percentage as with Young's modulus. At a grain percentage of 14% indicating the columnar structure due to the drawing process, the mean yield strength is 354 MPa. At a grain percentage of 16% after 100 °C annealing, the yield strength decreases slightly to 334 MPa. In the 200 °C-annealed wire showing the lowest recrystallized grain percentage, the yield strength is 295 MPa, only a 12% decrease from the value in the 100 °C-annealed wire. The other two wires obtained under the same annealing conditions have grain percentages of 38 and 55%, which lead to reductions in yield strength to 154 and 101 MPa, respectively. At a grain percentage of 100%, the strength reaches 98 MPa on average. We concluded that the large scatter of yield strength seen in the 200 °C-annealed wires in Fig. 5(b) is caused by the difference in the number of recrystallized grains in the wires.

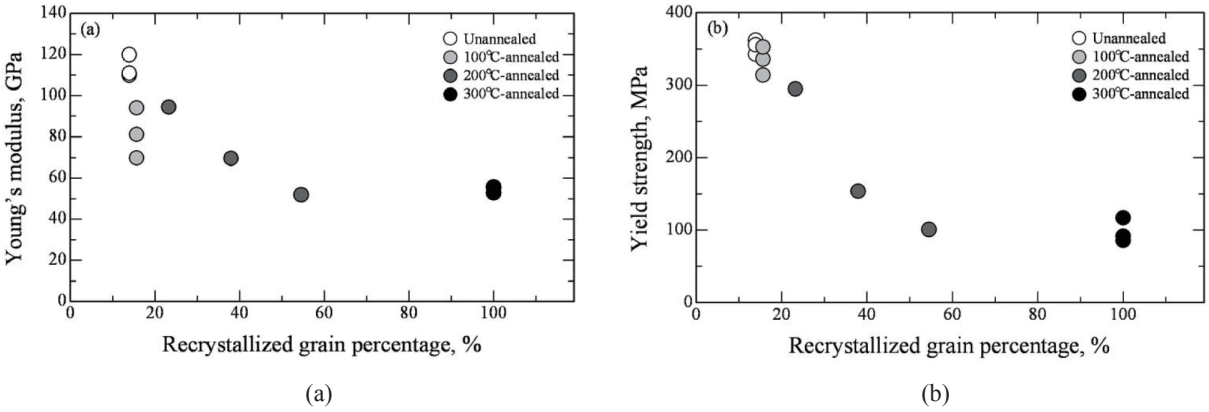

(a) (b)

Fig. 7. Effect of recrystallized grain percentage on mechanical properties of Au bonding wires: (a) Young's modulus and (b) yield strength.

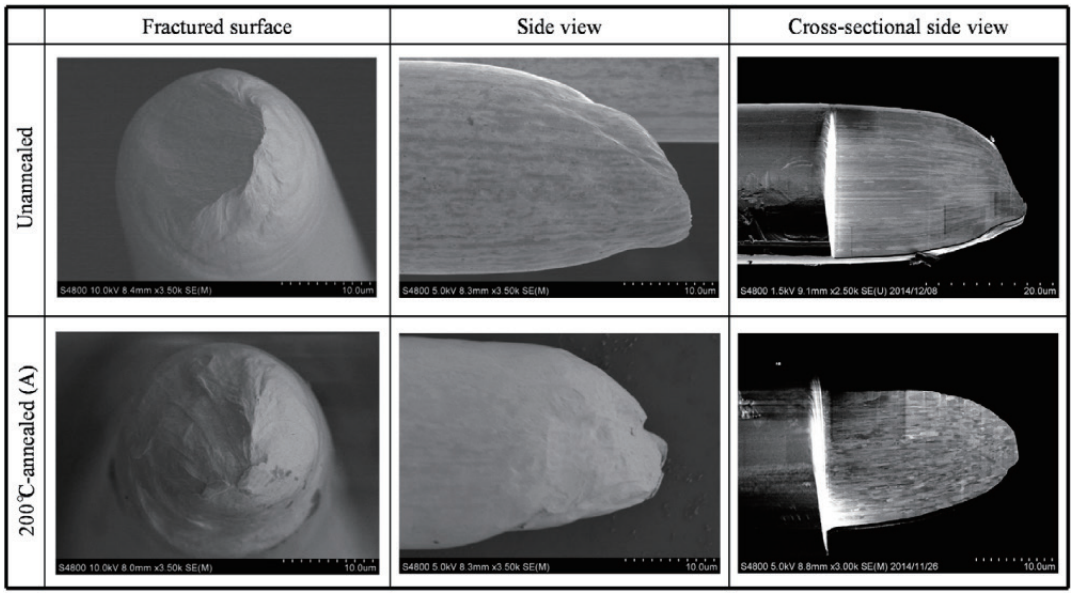

Fig. 8. SEM photographs of the fractured surface of the unannealed and 200 °C-annealed Au bonding wires.

Figures 8(a) and 8(b) show representative fracture surfaces of the unannealed and 200°C-annealed (A) wires, respectively. In the unannealed wire, necking occurs where the fracture is formed. A cup-and-cone-like fracture surface is obtained, which indicates that the wire experiences ductile fracture.[30] From the cross-sectional photograph produced by FIB fabrication, fibril-like crystal columns are concentrated toward the core; thereby, the relatively flat fractured face would have been formed at the tip. In the 200 °C-annealed (A) wire, it is confirmed that necking occurs before the fracture as with the unannealed wire. It is found, however, that the fracture surface is not a cup-and-cone-like surface, but a more acuate surface. Note that relatively large spherical grains can be seen in the vicinity of the necked portion, which clearly differs from what is observed in the unannealed wire. During local plastic deformation, crystal grain aggregation originating from relatively easy grain rotations could have occurred simultaneously with the segregation derived from dislocation slips in a grain. Since these two phenomena had probably happened repeatedly, the wires with recrystallized spherical grains would have shown a larger braking strain than the wires with crystal columns.

4. Conclusion

We investigated the effect of vacuum annealing on the tensile mechanical properties of Au bonding wires by quasi-static uniaxial tensile tests. The mean Young's modulus and yield strength for the unannealed wires were 114 GPa and 354 MPa, respectively, which were higher than those for the bulk. With increasing annealing temperature, the texture of Au bonding wires gradually changed, that is, the size and number of spherical crystal grains increased with an increase in annealing temperature. With an increase in spherical crystal grain percentage in the cross section, Young's modulus and yield strength gradually decreased. After annealing at 300 °C, these mean values were 55 GPa and 98 MPa, respectively.

The 200 °C-annealed wires showed a large scatter in both Young's modulus and yield strength. By cross-sectional observation, it was found that the difference in the degree of recrystallization, which was produced by annealing at a temperature very close to the recrystallization temperature for Au, gave rise to the scatter in the data.

References

1 S. K. Prasad: Advanced Wirebond Interconnection Technology (Kluwer Academic Publishers, Dordrecht, 2004).
2 F. D. Danaher, J. J. Williams, D. R. P. Singh, L. Jiang, and N. Chawla: J. Electr. Mater. **40** (2011) 1422.
3 D. S. Liu and Y. C. Chao: J. Electr. Mater. **32** (2003) 159.
4 M. F. M. Yunoh, S. Abdullah, A. Jalar, M. F. Rosle, and S. A. Radzi: J. Sci. Technol. **2** (2011) 121.
5 S. B. Son, H. Roh, S. H. Kang, H. S. Chung, Y. S. Choi, J. S. Cho, and K. H. Oh: Gold Bull. **44** (2011) 231.
6 K. S. Kim, J. Y. Song, E. K. Chung, J. K. Park, and S. H. Hong: Mech. Mater. **38** (2006) 119.
7 S. H. Kang, J. H. Cho, J. S. Hwang, J. S. Cho, Y. J. Park, J. T. Moon, and K. H. Oh: Mater. Sci. Forum **550** (2007) 289.
8 Y. Liu and W. K. Jones: J. Electr. Mater. **33** (2004) 929.
9 T. Namazu, Y. Nagai, N. Naka, N. Araki, and S. Inoue: J. Eng. Mater. Technol. **134** (2011) 011009.
10 M. Fujii, T. Namazu, H. Fujii, K. Masunishi, Y. Tomizawa, and S. Inoue: J. Vac. Sci. Technol. B **30** (2012) 031804.
11 T. Namazu, M. Fujii, H. Fujii, K. Masunishi, Y. Tomizawa, and S. Inoue: J. Microelectromech. Syst. **22** (2013) 1414.
12 T. Namazu, S. Inoue, H. Takemoto, and K. Koterazawa: IEEJ Trans. Sens. Micromach. **125** (2005) 374.
13 T. Namazu and S. Inoue: Fatigue Fract. Eng. Mater. Struct. **30** (2007) 13.
14 T. Namazu, H. Takemoto, H. Fujita, and S. Inoue: J. Sci. Technol. Adv. Mater. **8** (2007) 146.
15 T. Namazu, A. Hashizume, and S. Inoue: Sens. Actuators, A **139** (2007) 178.
16 T. Namazu, S. Inoue, K. Takio, T. Fujita, K. Maenaka, and K. Koterazawa: Proceedings of the 18th IEEE International Conference on Microelectromechanical Systems (2005) pp. 447–450.
17 Y. Nagai, T. Namazu, and S. Inoue: Surf. Interface Anal. **40** (2008) 993.
18 T. Namazu and Y. Isono: J. Microelectromech. Syst. **18** (2009) 129.
19 D. M. Schaefer, A. Patil, R. P. Andres, and R. Reifenberger: Appl. Phys. Lett. **63** (1993) 1492.
20 J. H. Cho, Y. W. Kim, K. H. Oh, J. S. Cho, J. T. Moon, J. Lee, and A. D. Rollett: Metall. Mater. Trans. A **34** (2003) 1113.
21 S. H. Kang, H. S. Jung, W. H. Bang, J. H. Cho, K. H. Oh, D. S. Kim, and S. H. Park: Mater. Sci. Forum **495** (2005) 907.
22 S. Tomiyama and Y. Fukui: Gold Bull. **15** (1982) 43.
23 W. Leszek: Image Analysis: Applications in Materials Engineering (CRC Press, Boca Raton, 1998).
24 B. Wu, A. Heidelberg, and J. J. Boland: Nat. Mater. **4** (2005) 525.
25 J. H. Seo, Y. Yoo, N. Y. Park, S. W. Yoon, H. Lee, S. Han, and J. P. Ahn: Nano Lett. **11** (2011) 3499.
26 F. Wang, Y. Dai, J. Zhao, Q. Li, and B. Zhang: J. Nanopart. Res. **16** (2014) 1.
27 H. D. Espinosa and B. C. Prorok: J. Mater. Sci. **38** (2003) 4125.
28 N. Karanjgaokar, K. Jonnalagadda, I. Chasiotis, J. Chee, A. Mahmood, and D. Peroulis: Society for Experimental Mechanics—11th International Congress and Exhibition on Experimental and Applied Mechanics (2008) Vol. 4, pp. 1860–1866.
29 S. J. Lee, S. W. Han, S. M. Hyun, H. J. Lee, J. H. Kim, and Y. I. Kim: Curr. Appl. Phys. **9** (2009) 75.
30 Y. H. Kwon, H. J. Seol, H. I. Kim, K. J. Hwang, S. G. Lee, and K. H. Kim: J. Biomed. Mater. Res. Part B: Appl. Biomater. **73** (2005) 285.